



32101 022039877

# DELAMINATION *R*-CURVE PHENOMENA DUE TO DAMAGE

Z. SUO, G. BAO† and B. FAN†

Mechanical Engineering Department, University of California, Santa Barbara, CA 93106, U.S.A.

(Received 24 September 1990; in revised form 18 December 1990)

## ABSTRACT

RESISTANCE to delamination in composites can be enhanced by a variety of bridging mechanisms. The bridging zone size is usually several times the lamina thickness, so it is questionable to think of delamination resistance as a material property independent of specimen size and geometry. When measured with slender beams, the plateau resistance is found to be independent of the beam thickness. However, the steady-state bridging zone size increases with the beam thickness. Further implications of the large-scale bridging are studied using a family of steady-state, mixed-mode delamination beams, in conjunction with an idealized damage response. The complete solution is obtained for the model, which allows the *R*-curves to be constructed for given model parameters. The significance of the steady-state cracking, which is crucial in understanding delamination *R*-curves, is elucidated by contrasting double-cantilever beams loaded by moments and by wedge forces. As an inverse process, it is recommended that *R*-curves be used as an experimental probe to study localized damage response, such as polymer craze and interface separation.

## 1. INTRODUCTION

OVER THE last decade, it has been increasingly evident that the toughness of brittle materials can be enhanced by bridging mechanisms. The mechanics language that describes this is resistance curves (*R*-curves): toughness increases as a crack grows. Many material systems have been tested and modeled. In polycrystalline ceramics, grains that cross over the crack faces are responsible for the toughness much higher than the surface energy of the corresponding crystals (VEKINIS *et al.*, 1990). Bridging in ceramics can also be supplied by reinforcements such as high-strength fibers, metal particles and networks. A perspective for these toughening approaches is provided by EVANS (1990). The *R*-curve behaviors are discovered in metallic adhesive joints, where much energy is absorbed by periodic arrays of cavities growing under constrained plastic flow, and the intact metal patches provide the closure force (REIMANIS and EVANS, 1990; VARIAS *et al.*, 1990). Such cavities can also be etched on the substrate surfaces prior to bonding (OH *et al.*, 1988). For ceramic powder compacts in the green state, fracture resistance largely originates from bridging particles.

Attention here is focussed on the delamination of unidirectional or laminated composites. A comparative literature study shows that, for both polymer and ceramic matrix composites, bridging is usually due to unbroken fibers left behind the crack front, while the crack switches from one fiber-matrix interface to another as it

† Permanent address: Department of Mechanical Engineering, The Johns Hopkins University, Baltimore, MD 21218, U.S.A.

(ST)  
TA350  
568

~~(SA)~~  
505

1

32101-022039877

vol. 40, no. 1-4

propagates (LUCAS and ODEGARD, 1990; SBAIZERO *et al.*, 1990). Additional resistance for polymer matrix composites comes from damage in the form of voids, craze or micro-cracks (CHAI, 1988; BRADLEY, 1989; SU, 1990). Three-dimensional architecture of threading fibers can also give rise to substantial fracture resistance (BYUN *et al.*, 1990). Impressive micrographs showing various damage behaviors can be found in these papers.  $R$ -curves have been measured for several polymer and ceramic laminates, e.g. DE CHARENTENAY *et al.* (1984), HASHEMI *et al.* (1990), and SPEARING and EVANS (1990).

In contrast to atomic cohesion that occurs over a multiple of the lattice spacing with huge stresses, most bridging mechanisms are characterized by small stresses (5 MPa, say) operating over a large separation (0.1 mm, say). Consequently, as a prerequisite to significant toughening, a large-scale bridging zone must develop ahead of the pre-cut. In laminates, the fiber bridging zone length is typically several times the lamina thickness. From the viewpoint of material characterization,  $R$ -curves are no longer a material property, since they depend on specimen size and geometry. We favor an approach that regards the bridging response, a homogenized nonlinear traction-separation law, as a basic material property. The law can be obtained by either modeling or testing with laboratory samples, and subsequently used as input data to predict the response of more complicated structures.

Large-scale bridging concepts have been explored by MAI and LAWN (1986), ZOK and HOM (1990), and BAO *et al.* (1990). Studies up to date have suffered from the complexities caused by specimen geometries, mode mixity and damage response. The intent of this paper is to investigate the delamination resistance using simple, yet representative, specimens and damage response. Several generic features unique to delamination  $R$ -curves are identified. Experimental procedures are proposed to infer the bridging law from the testing data.

## 2. BASIC MECHANICS

### 2.1. *A family of steady-state, mixed-mode delamination beams*

Consider a beam with a pre-cut, loaded at the edges by moments or axial forces (Fig. 1). Owing to the symmetry, mode I and mode II can still be unambiguously defined under the large-scale bridging: the loadings that do not induce sliding are mode I [Fig. 1(a)], and the loadings that do not induce opening are mode II [Figs 1(b) and (d)]. A mixed mode is obtained by superposition of the four basic loadings [see also Fig. 1(c)]. Examples include four-point flexure and crack-lap-shear. A more general family of steady-state delamination specimens with cracks off the centerline in orthotropic materials has been analyzed in SUO (1990). To elucidate the basic mechanics, mode I is discussed in this and the next section. Mode II and the mixed mode will be studied in Section 4.

The damage is assumed to be localized in a planar zone ahead of the pre-cut front, to be consistent with the experimental observations for most brittle matrix composites. The damage zone size  $L$  can be comparable to, or larger than, the beam thickness  $h$ , but the pre-cut and beam are much longer, so that the geometry is fully characterized

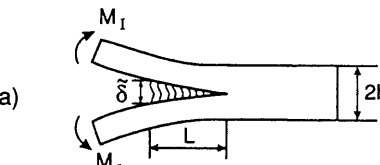
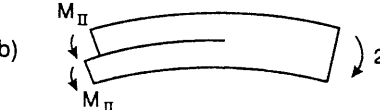
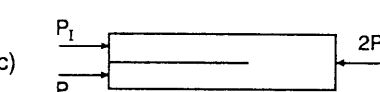
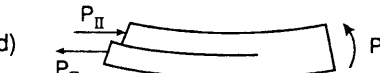
Specimen	$\frac{E}{1-\nu^2} \mathcal{G}_I$	$\frac{E}{1-\nu^2} \mathcal{G}_{II}$
	$12M_I^2 h^{-3}$	0
	0	$9M_{II}^2 h^{-3}$
	0	0
	0	$\frac{1}{4} P_{II}^2 / h$

FIG. 1. Family of delamination beams. The damage zone is an additional energy dissipater. The geometry is specified by  $L/h$ . Mixed-mode loadings can be obtained by the superposition of these basic cases.

by the ratio  $L/h$ . In Fig. 1(a), the *global* energy release rate equals the *J*-integral over the external boundary, and measures the magnitude of the applied load (RICE, 1968):

$$\mathcal{G} = CM^2, \quad C = 12(1-\nu^2)/Eh^3, \quad (1)$$

where  $M$  is the applied moment per unit width,  $C$  the beam compliance,  $2h$  the thickness,  $E$  the Young's modulus, and  $\nu$  the Poisson's ratio. The material is assumed to be elastically isotropic and homogeneous, and plane strain conditions prevail. The subscript I indicating mode I is dropped. Observe that  $\mathcal{G}$  does not depend on the crack size, nor on the damage zone (size, constitutive law, etc.). This prominent feature suggests an experimental procedure to measure the damage response, as will be described at the end of this section.

The pure moments, for example, can be applied to arms bonded to beams, a design that has been used for electronic ceramics (POHANKA and SMITH, 1988). Other specimens that feature the steady state include double torsion (VEKINIS *et al.*, 1990), four-point flexure (CHARALAMBIDES *et al.*, 1989), edge delamination (O'BRIEN, 1987), and a bilayer held in rigid grips (LIECHTI and CHAI, 1990). They are all suitable for *R*-curve measurement.

## 2.2. Essential features of delamination $R$ -curves

Phenomenological delamination  $R$ -curves are shown schematically in Fig. 2. Focus on a  $R$ -curve of a given beam thickness, say,  $h_1$ . The specimen can sustain the increasing moment, without appreciable damage ahead the pre-cut front, up to a critical point corresponding to  $\mathcal{G}_0$ . Subsequently, the damage zone size  $L$  increases with the applied moment  $M$ , leading to an increasing curve of resistance  $\mathcal{G}_R$ . The damage zone may attain a steady state: it maintains a self-similar opening profile and a constant length  $L_{ss}$ , translating in the beam, leaving behind the crack faces free of traction. Correspondingly, a plateau,  $\mathcal{G}_{ss}$ , would appear on the  $R$ -curve. We observe that the steady-state large-scale bridging is unique to the slender beams. Most other specimens, such as edge-notched specimens, do not admit the steady state when the bridging zone is comparable to the specimen size. As a convention, the current crack front is identified with the damage front, and therefore the  $R$ -curve is the same as the  $\mathcal{G}_R$ - $L$  plot. For the fiber cross-over, the damage front is indeed the crack tip, and can be observed in experiments. But, for ductile damage, this convention may cause ambiguity in experiments, and much care is demanded.

To proceed further, the DUGDALE (1960) model is invoked, which, in its generalized form, simulates the homogenized damage response with an array of continuously distributed, nonlinear springs. Specifically, at each point in the damage strip, the closure traction  $\sigma$  depends locally on the separation  $\delta$ :

$$\sigma = \sigma(\delta). \quad (2)$$

The functional form is specific to the damage, but is assumed to be *identical* for every point in the damage strip, and *independent* of the specimen geometry. A maximum separation  $\delta_0$  exists, beyond which the closure traction vanishes. The spring laws may be measured or modeled using simplified systems [e.g. ASHBY *et al.* (1989), BAO and HUI (1990), BUDIANSKY *et al.* (1988), and EVANS (1990)]. They can also be inferred from experimental  $R$ -curves. The latter is the major theme of this paper.

The following energy balance is due to the  $J$ -integral conservation (RICE, 1968):

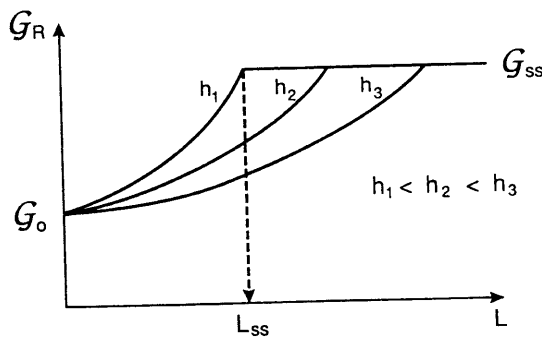


FIG. 2. Two generic features of delamination  $R$ -curves. The plateau  $\mathcal{G}_{ss}$  is independent of the beam thickness  $h$ . The steady-state damage zone size  $L_{ss}$  increases with  $h$ .

$$\mathcal{G} = \mathcal{G}_0 + \int_0^{\tilde{\delta}} \sigma(\delta) d\delta, \quad (3)$$

where  $\tilde{\delta}$  is the end-opening of the damage zone, or the separation at the pre-cut tip. We will not distinguish the driving force  $\mathcal{G}$  and the resistance  $\mathcal{G}_R$  hereafter, as they can be judged from the context.  $\mathcal{G}$  indicates the applied load level as shown in (1), and  $\mathcal{G}_0$  is the energy dissipated at the damage front. They will be referred to as the *global* and the *local*, respectively. The difference in (3) is the energy to create the damage. The steady-state resistance  $\mathcal{G}_{ss}$  is attained when the end-opening reaches the critical separation,  $\tilde{\delta} = \delta_0$ . Thus, from (3)  $\mathcal{G}_{ss}$  equals the sum of  $\mathcal{G}_0$  and the area under the  $\sigma(\delta)$  curve. The plateau  $\mathcal{G}_{ss}$  does not depend on the beam thickness, and is therefore a property for a given laminate.

But how long will the damage strip develop before the steady state is attained? The steady-state bridging zone size,  $L_{ss}$ , indicates the *quality* of a bridging mechanism: toughness gained from too long a damage strip may not be useful in practice. From other perspectives, however, a long damage zone might be desirable. For example, the larger scales may help the experimental studies of damage response. Both the bridging mechanism and the specimen geometry affect  $L_{ss}$ . Bridging mechanisms with small closure stress operating over a large separation result in a large  $L_{ss}$ . A thicker, stiffer, beam is more constrained against deflection, and thus exhibits a larger  $L_{ss}$ . The latter is indicated in Fig. 2. These features are independently observed in an experiment with a unidirectional ceramic composite by SPEARING and EVANS (1990).

Equation (3) suggests an experimental procedure to determine the damage response. By continuously measuring the end-opening  $\tilde{\delta}$ , together with the  $R$ -curve, the spring law is given by

$$\sigma(\tilde{\delta}) = \partial \mathcal{G}_R / \partial \tilde{\delta}. \quad (4)$$

This is obtained by differentiating (3). The intrinsic resistance  $\mathcal{G}_0$  is assumed to be independent of the damage accumulation. This method by-passes the complexities of large-scale bridging. However, this method is *not* applicable for specimens that do not admit the steady state. For those specimens,  $\mathcal{G}_R$ , the  $J$ -integral over the external boundary, depends on the details of the bridging law, and therefore can only be calculated after the law is known. Further discussions are given in Section 5. Large-scale bridging may serve as an experimental probe for studying localized (planar) damage response, such as polymer craze and interface separation, when uniform separation over a sample is difficult to accomplish due to the instabilities triggered by inhomogeneities and softening (SUO *et al.*, 1990).

### 3. OPENING MODE $R$ -CURVES

To gain quantitative insight, we analyze an idealized damage response shown in Fig. 3. The closure traction  $\sigma$  is related to the separation  $\delta$  via

$$\sigma = \sigma_0 + S\delta, \quad (5)$$

where  $S$  is the spring stiffness, and  $\sigma_0$  the yield stress. A limit separation,  $\delta_0$ , is specified

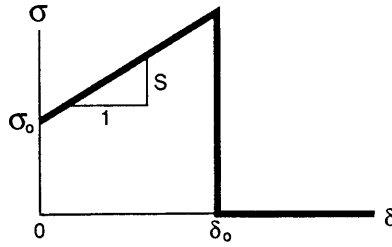


FIG. 3. Three-parameter damage response.

to represent the reinforcement necking or fiber breakage, so that the closure stress vanishes when  $\delta > \delta_0$ . This three-parameter response embodies models representative of a variety of damage behaviors. For example,  $S = 0$  gives the rigid plasticity typical of ductile reinforcements. Hardening and softening are represented by  $S > 0$  and  $S < 0$ , respectively. Linear springs are recovered by  $\sigma_0 = 0$ .

The energy balance (3) becomes

$$\mathcal{G} = \mathcal{G}_0 + \sigma_0 \tilde{\delta} + S \tilde{\delta}^2 / 2. \quad (6)$$

The plateau resistance  $\mathcal{G}_{ss}$  is obtained when  $\tilde{\delta} = \delta_0$ . A key nondimensional parameter is the effective stiffness ratio of the spring to the beam:

$$\Sigma = SL^4C. \quad (7)$$

### 3.1. General solution

The nonlinear spring law (5) is analogous to that for residual stress problems, and can be treated by an Eshelby-type superposition (Fig. 4). The problem in Fig. 4(a) is trivial: displacement is everywhere zero, and the only nonzero stress is in the spring, being  $\sigma_0$ . The coupled spring-beam system in Fig. 4(b) is *purely linear*, so that  $\tilde{\delta}$  and  $\sqrt{\mathcal{G}_0}$  are linear in  $\sigma_0$  and  $M$ :

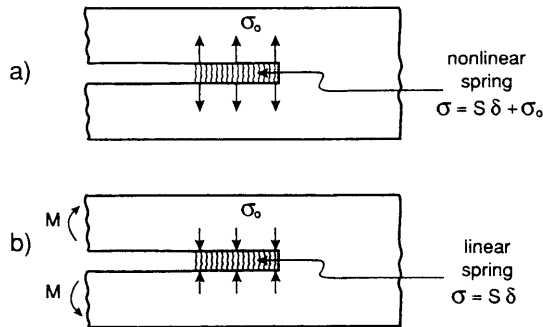


FIG. 4. Eshelby-type superposition procedure to reduce the nonlinear system to a pure linear spring-beam.

$$\tilde{\delta} = a_1 L^2 CM - a_2 L^4 C \sigma_0, \quad (8a)$$

$$\sqrt{g_0} = a_3 \sqrt{CM} - a_4 L^2 \sqrt{C} \sigma_0. \quad (8b)$$

A somewhat arbitrary normalization is chosen so that the  $a$ s are dimensionless. These coefficients should be determined by solving the elasticity problem rigorously.

It can be shown that  $a_i$  depends only on  $L/h$  and  $\Sigma$ . The amount of calculation was significantly reduced once we noticed three relations:

$$a_4 = a_1/2, \quad a_3 = (1 - \Sigma a_1^2/2)^{1/2}, \quad a_2 = (1 - a_3)/\Sigma. \quad (9)$$

Thus, once  $a_1$  is known, so are the other three coefficients. These relations are derived by substituting (8) into (6); the result is a quadratic in  $\sigma_0$  and  $M$  being identically zero. This in turn implies that all three terms in the quadratic vanish, leading to (9).

The coupled beam-spring system in Fig. 4(b) with  $M \neq 0$  but  $\sigma_0 = 0$  is analyzed with over 300 runs of a finite-element analysis, within the applicable parameter regime. The computed coefficient  $a_1$ , depending on  $\Sigma$  and  $L/h$  only, is fitted by

$$\begin{aligned} a_1 &= A \exp[-B\Sigma(\Sigma + \Sigma_0)^{-1/2}], \\ A &= 1 + 1.325(h/L) + 0.35(h/L)^2, \\ B &= 0.353 + 0.374(h/L) + 0.373(h/L)^2 - 0.23(h/L)^3, \\ \Sigma_0 &= 6.127 \exp[-2.586(h/L) + 0.564(h/L)^2]. \end{aligned} \quad (10)$$

Figure 5 plots the finite-element data points and the fitting curves for  $a_1$ .

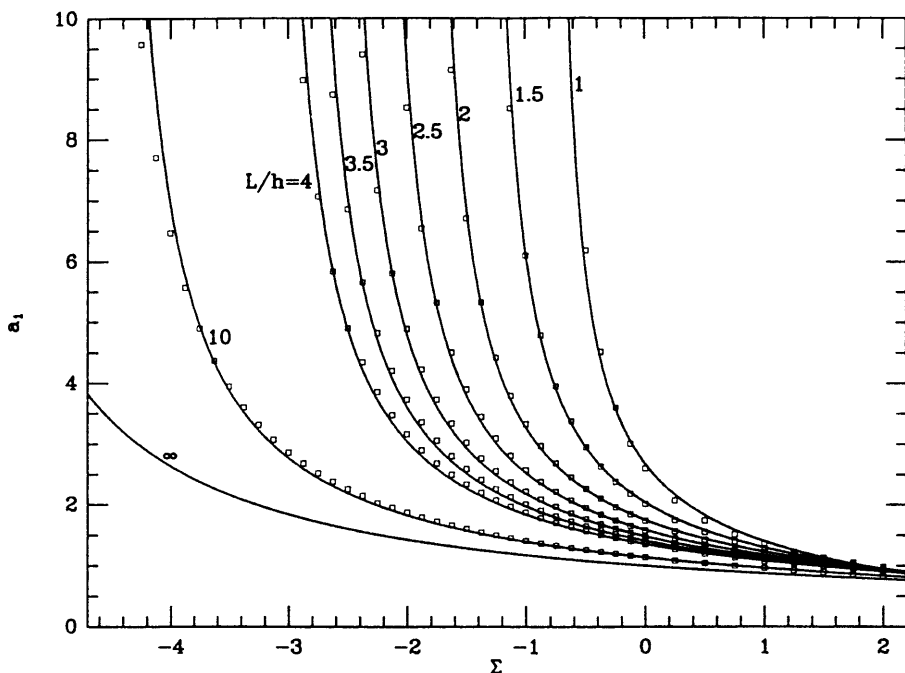


FIG. 5. Finite-element results and fitting curves for  $a_1$ .

In summary, (6)–(10) are all one needs to construct  $R$ -curves when the model parameters are known [mathematically, only two among (6), (8a) and (8b) are independent]. Specifically, the  $R$ -curve, the  $\mathcal{G}$ – $L$  plot, is given by (8b), with  $M$  related to  $\mathcal{G}$  via (1). With  $\tilde{\delta} = \delta_0$ ,  $\mathcal{G}_{ss}$  is determined by (6), and  $L_{ss}$  from (8a). These can be coded with a short computer program. Special cases will be discussed in the next two subsections to gain a quantitative feel. Below we digress to present a few interesting results.

The *exact* asymptote as  $L/h \rightarrow \infty$  is obtained using the classical theory of beams on elastic foundations [e.g. DEN HARTOG (1987)]:

$$a_1(\Sigma) = \begin{cases} \frac{\cosh^2 \xi - \cos^2 \xi}{\xi^2 (\cosh^2 \xi + \cos^2 \xi)}, & \xi = (\Sigma/2)^{1/4}, \quad \Sigma > 0, \\ \frac{2 \sinh \xi \sin \xi}{\xi^2 (1 + \cosh \xi \cos \xi)}, & \xi = (-2\Sigma)^{1/4}, \quad \Sigma < 0. \end{cases} \quad (11)$$

Only positive spring stiffness is considered in the book, but a slight modification solves the softening springs. This asymptote is plotted on Fig. 6. Note that infinite and negative deflections appear for softening springs. The first instability occurs at  $\Sigma \approx -6.181$ . A similar behavior appears for finite  $L/h$ , but, for the present problem, only the results up to the first instability for each  $L/h$  are reported in Fig. 5.

Below we derive an approximate relationship between  $L_{ss}$  and  $h$ , which indicates that  $L_{ss}$  indeed increases with  $h$ . At the steady state, except for  $a_1$ ,  $a_2$  and  $L^4 C$ , all

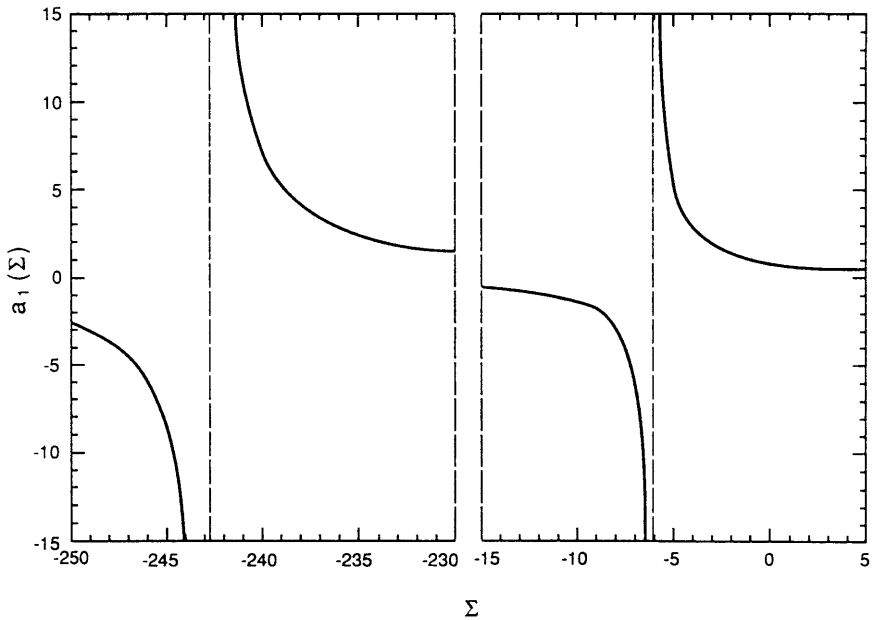


FIG. 6. Plot of  $a_1(\Sigma, L/h = \infty)$ . Infinitely many instability points exist in the regime  $\Sigma < 0$ . Only the first two are shown.



other quantities in (8a) are material parameters. For fixed  $\Sigma$ ,  $a_1$  does not vary significantly for large  $L/h$ , neither does  $a_2$  due to (9). Hence the combination  $L^4 C$  solved from (8a) is almost independent of  $h$ , so that for a given composite

$$L_{ss} \propto C^{-1/4} \quad \text{or} \quad L_{ss} \propto h^{3/4}. \quad (12)$$

The relation becomes accurate for large  $L_{ss}/h$ . This strong thickness dependence is observed in experiments with a unidirectional ceramic composite (SPEARING and EVANS, 1990).

### 3.2. Rigid plastic bridging

Two examples are given to illustrate how the theoretical results contained in this paper can be used, in conjunction with experimental  $R$ -curves, to characterize composites. It is appreciated that  $R$ -curves themselves are not adequate to characterize materials, since they are specimen-dependent. But they contain the information on model parameters, such as yield stress, maximum separation and stiffness, which can be regarded as material properties. The strategy is to extract these parameters from the experimental  $R$ -curves, and use them as part of the material data base to predict structural behaviors.

Consider first the case  $S = 0$  suitable for ductile reinforcements. The response is specified by two parameters: the yield stress  $\sigma_0$ , and the maximum separation  $\delta_0$ . The steady-state toughness is given by

$$\mathcal{G}_{ss} = \mathcal{G}_0 + \sigma_0 \delta_0. \quad (13)$$

With  $\Sigma = 0$ , (8) takes the limit

$$\tilde{\delta} = a_1 L^2 \sqrt{C\mathcal{G}} - \frac{a_1^2}{4} L^4 C \sigma_0, \quad (14a)$$

$$\sqrt{\mathcal{G}} = \sqrt{\mathcal{G}_0} + \frac{a_1}{2} \sqrt{CL^2 \sigma_0}. \quad (14b)$$

Now  $a_1$  equals  $A$  in (10).

The quantities  $\mathcal{G}_0$ ,  $\mathcal{G}_{ss}$  and  $L_{ss}$  can usually be measured from fracture tests. Using these, the model parameters  $\sigma_0$  and  $\delta_0$  can be inferred from (13) and (14). To gain some feel for the magnitude,  $R$ -curves defined by (14b) are plotted in Fig. 7 in a dimensionless form. The plateau  $\mathcal{G}_{ss}$  in (13) should be a horizontal line independent of  $h$  and  $L$  (not shown in Fig. 7).

### 3.3. Softening bridging

The case  $S < 0$  is thought to be appropriate to represent the fiber cross-over. As the crack opens, the fibers are peeled off from the matrix, and the closure traction diminishes. The negative stiffness depends on the number of the cross-over fibers, and on the adhesion between the fibers and the matrix. Our model is specified by two parameters  $\sigma_0$  and  $\delta_0$ , with  $S = -\sigma_0/\delta_0$  (inset of Fig. 8). The model is also applicable

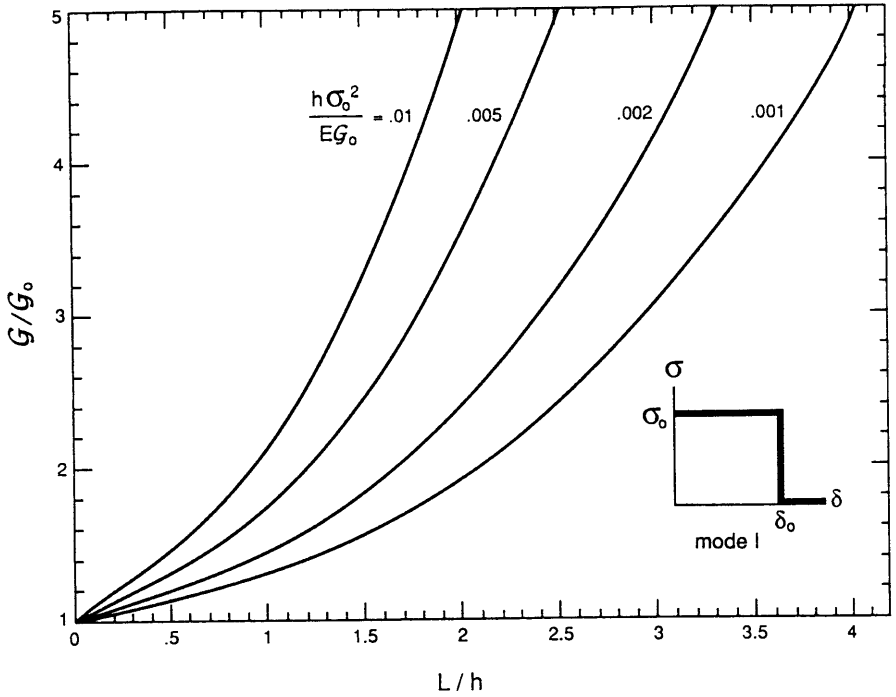


FIG. 7. Dimensionless  $R$ -curves predicted using the rigid plastic damage response (mode I).

for debonding ductile reinforcements (BAO and HUI, 1990). The plateau resistance is given by

$$\mathcal{G}_{ss} = \mathcal{G}_0 + \frac{1}{2}\sigma_0\delta_0. \quad (15)$$

The  $R$ -curves are given by (8b) once the model parameters are given.

Now we focus on the inverse problem: how to infer  $\sigma_0$  and  $\delta_0$  if an  $R$ -curve has been measured. With  $\mathcal{G}_0$  and  $\mathcal{G}_{ss}$  read from the  $R$ -curve, (15) gives the product  $\sigma_0\delta_0$ . to determine  $S$ , (8) is specialized at the steady state:

$$\mathcal{G}_{ss}/\mathcal{G}_0 = a_3^2. \quad (16)$$

This equation is plotted on Fig. 8. With  $L_{ss}$  also read from the  $R$ -curve,  $S$  can be obtained from the plot. This procedure is currently being used in the experiment by SPEARING and EVANS (1990).

#### 4. MODE II AND MIXED-MODE $R$ -CURVES

##### 4.1. Pure mode II

Now  $\delta$  represents the crack sliding, and  $\sigma$  the shear traction that opposes the sliding. The three-parameter damage response in Fig. 3 is assumed. Consider first the loading case in Fig. 1(b). The mode II global energy release rate is

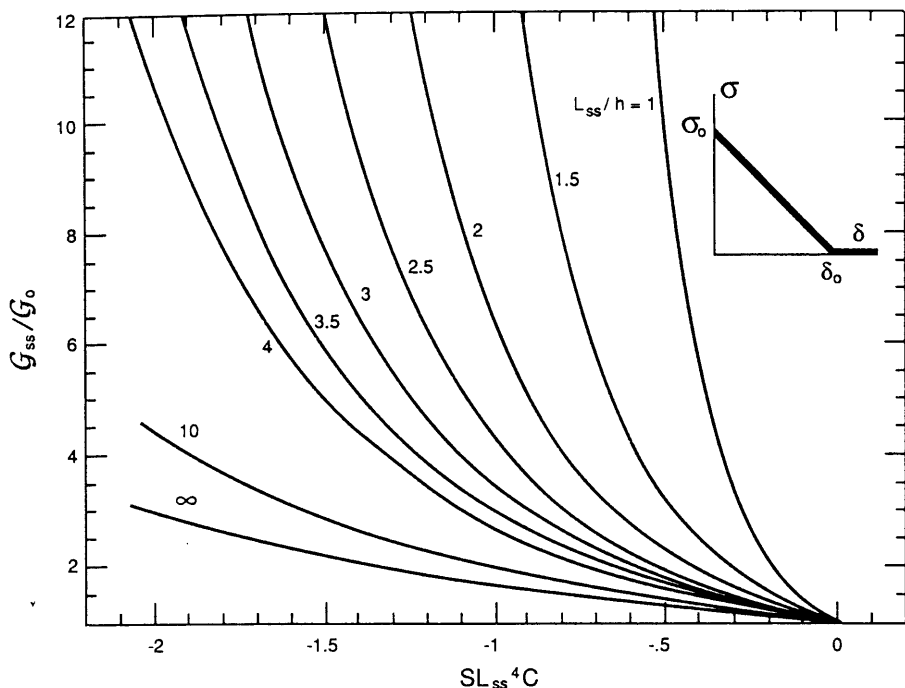


FIG. 8. Insert shows a two-parameter softening damage response. The plot is used to infer the negative spring stiffness  $S$ . With  $\mathcal{G}_{ss}$ ,  $\mathcal{G}_0$  and  $L_{ss}$  from an  $R$ -curve,  $S$  can be read from this plot.

$$\mathcal{G} = DM^2, \quad D = 9(1 - \nu^2)/Eh^3. \quad (17)$$

The conservation of the  $J$ -integral (6) still applies, which connects the global and local energy release rates with the *end-sliding*,  $\tilde{\delta}$ . Linearity and dimensionality imply that

$$\begin{aligned} \tilde{\delta} &= b_1 Lh \sqrt{D} \sqrt{\mathcal{G}} - b_2 L^2 h^2 D \sigma_0, \\ \sqrt{\mathcal{G}_0} &= b_3 \sqrt{\mathcal{G}} - b_4 Lh \sqrt{D} \sigma_0. \end{aligned} \quad (18)$$

The dimensionless coefficients  $b_i$  depend on  $L/h$  and  $\Sigma' = SL^2 h^2 D$  only. Relationships in (9) are still valid for the  $b_s$ , with  $\Sigma$  replaced by  $\Sigma'$ . For a given material, it can be shown that  $L_{ss} \propto h^{1/2}$  is approximately valid for large  $L_{ss}/h$ .

For the loading case in Fig. 1(d), the energy release rate is

$$\mathcal{G} = \frac{1}{4}(1 - \nu^2)P^2/Eh. \quad (19)$$

Equation (18) still applies, with identical  $b_s$ . This is because  $b_2$  and  $b_4$  are coefficients related to  $\sigma_0$  alone, and because (9) is valid for both moments and axial forces. Consequently, the  $R$ -curves are identical for the loadings in Figs 1(b) and (d). The same is true for any linear combinations of the two loadings. This remarkable conclusion results from the simple damage response we have assumed here, but might be valid approximately for arbitrary damage response.

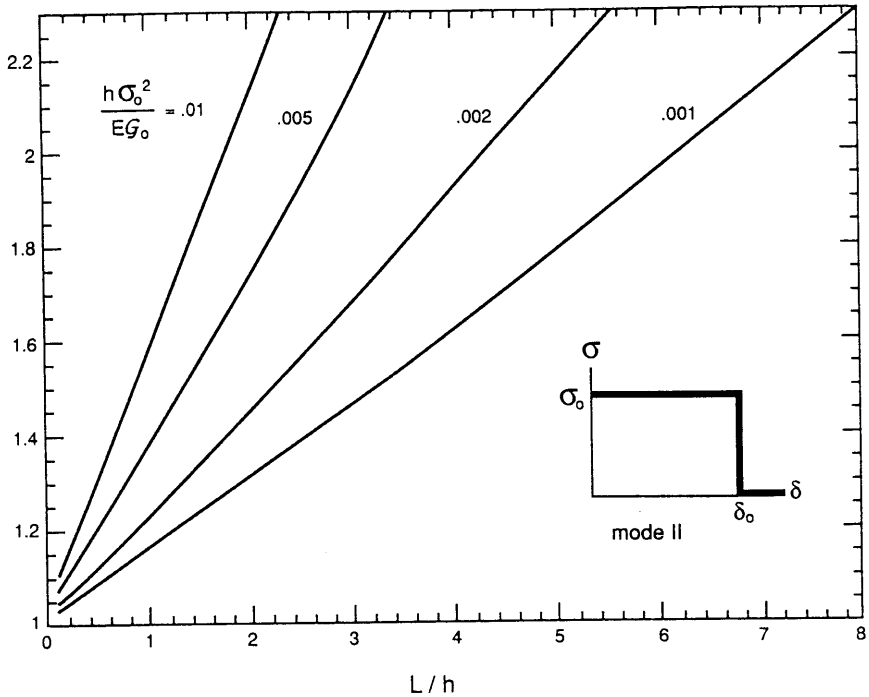


FIG. 9. Dimensionless  $R$ -curves predicted using the rigid plastic damage response (mode II).

For rigid plastic springs ( $S = 0$ ), (9) reduces to  $b_2 = b_1^2/4$ ,  $b_3 = 1$ ,  $b_4 = b_1/2$ . The coefficient  $b_1$  is extracted by solving the boundary value problem with finite elements, and the results are fitted by

$$b_1 = \frac{4}{3} + 0.28 \frac{h}{L}. \quad (20)$$

The error is less than 1% when  $L/h > 0.5$ . Dimensionless  $R$ -curves are plotted in Fig. 9. A comparison with Fig. 7 shows that a much longer damage zone is typically needed for mode II than mode I to attain the same level of toughening. This is consistent with the experimental observations of BRADLEY (1989) with unidirectional polymer composites.

#### 4.2. Mixed mode

Mixed-mode specimens can be obtained by the superposition of the basic loadings in Fig. 1. Consider a simple case that the spring laws are decoupled: opening does not induce shear traction, and *vice versa*. While this damage response cannot be defended rigorously on a physical basis, it does shed some insight into the subject. The  $R$ -curves for the two modes are independent of each other, and each evolves in accordance with the mode I or mode II as computed previously. Ambiguity exists to

specify the mode mixity: the local mode mixity,  $\mathcal{G}_{110}/\mathcal{G}_{10}$ , is in general different from the global mode mixity,  $\mathcal{G}_{11}/\mathcal{G}_1$ , since toughening ratios for the two modes are different. The lengths over which the separation and sliding bridging operate are not necessarily the same.

Another situation can be treated readily. Let  $\delta_y$  and  $\delta_x$  be the opening and sliding displacements across the crack, and  $\sigma_y$  and  $\tau_{xy}$  be the normal and shear tractions opposing the crack growth. Suppose that the bridging response can be described by a displacement potential  $\phi(\delta_y, \delta_x)$ , such that

$$d\phi = \sigma_y d\delta_y + \tau_{xy} d\delta_x, \quad \phi(0, 0) = 0. \quad (21)$$

An application of the  $J$ -integral gives

$$\mathcal{G} = \mathcal{G}_0 + \phi(\tilde{\delta}_y, \tilde{\delta}_x). \quad (22)$$

Here  $\tilde{\delta}_y$  and  $\tilde{\delta}_x$  are the opening and sliding at the pre-cut tip, and  $\mathcal{G}_0$  is the energy dissipated at the damage fronts (note the opening front can be different from the sliding front). For the special case that  $\mathcal{G}_0 = 0$ , (22) suggests an experimental procedure to determine the potential  $\phi$  by measuring the delamination resistance  $\mathcal{G}$  and the opening and sliding at the pre-cut tip.

## 5. MOMENTS VS FORCES

Figure 10 illustrates a double-cantilever beam loaded by a wedge force,  $P$ , per unit width. This is a specimen with *no* steady state, and a contrast will be made between pure moments and wedge forces to elucidate the complexity. The  $J$ -integral over the external boundary now depends on the crack length and the details of the damage zone, which can only be obtained after the coupled, nonlinear spring-beam system is analyzed. This is not convenient in practice, and probably not meaningful for material characterization. Instead, as a convention, the load is converted to the nominal energy release rate as if the damage zone were absent, and the fictitious crack front coincides with the damage front. An accurate calibration for the double-cantilever beam *without* damage is given by WIEDERHORN *et al.* (1968)

$$\mathcal{G} = C(Pl)^2(1 + 0.677h/l)^2. \quad (23)$$

When damage is present, this  $\mathcal{G}$  does *not* equal the  $J$ -integral over the external boundary. Consequently, (3) does not apply here.

To illustrate a few points, the rigid plastic response is analyzed. The linear superposition of the stress intensity factors gives

$$\sqrt{\mathcal{G}} = \sqrt{\mathcal{G}_0} + \frac{a_1}{2} \sqrt{CL^2 \sigma_0}. \quad (24)$$

This is identical to (14b), with the same coefficient  $a_1$  provided that  $(l-L)$  exceeds a few times  $h$ . Thus the  $R$ -curves due to the incipient damage (i.e.  $\tilde{\delta} < \delta_0$ ) are identical to those for pure moments in Fig. 7.

The end-opening is

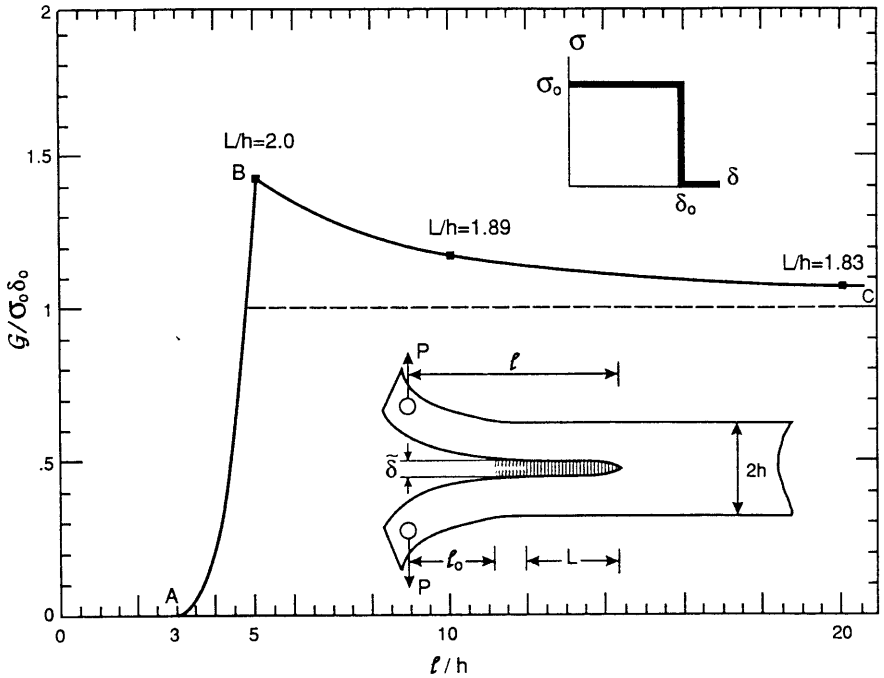


FIG. 10. Insert shows a double-cantilever beam loaded by wedge force. An  $R$ -curve consists of two stages: incipient damage  $AB$  when  $\tilde{\delta} < \delta_0$  and fully developed damage  $BC$  when  $\tilde{\delta} = \delta_0$ .

$$\tilde{\delta} = cL^2\sqrt{C\mathcal{G}} - \frac{a_1^2}{4}L^4C\sigma_0. \quad (25)$$

Compared with (14a), the coefficient  $c$  (not presented in the paper) now depends on  $l/h$  and  $L/h$ , and is determined by the deflection due to wedge forces instead of moments.

No steady-state is anticipated, since the translation self-similarity does not exist for the wedge force loading. The fracture resistance  $\mathcal{G}$  and the damage zone size  $L$  keep changing as the damage strip translates in the beam, maintaining  $\tilde{\delta} = \delta_0$ , and should be solved from (24) and (25) as a set of nonlinear algebraic equations.

Consider model parameters and specimen geometry specified by

$$\frac{\mathcal{G}_0}{\sigma_0\delta_0} = 0, \quad \frac{(1-\nu^2)h\sigma_0}{\delta_0 E} = 0.099, \quad \frac{l_0}{h} = 3, \quad (26)$$

where  $l_0$  is the initial crack size. The  $R$ -curve is plotted in Fig. 10, together with the pure-moment result  $\mathcal{G}_{ss} = \delta_0\sigma_0$  (the dashed line). Curve  $AB$  corresponds to the incipient stage  $\tilde{\delta} < \delta_0$ , and curve  $BC$  corresponds to  $\tilde{\delta} = \delta_0$ . The damage zone size  $L/h$  is also indicated at three points. Observe that both  $\mathcal{G}$  and  $L$  decrease as the damage strip translates. The nominal resistance thus determined *overestimates* what would be

experienced by a real delamination typically under a steady-state driving force. However, Fig. 10 shows that these deviations are insignificant if  $l/h$  is sufficiently large and  $L/h$  small.

The above conclusions are broadly consistent with the experimental findings with a unidirectional glass-epoxy composite, where fiber bridging was observed (PREL *et al.*, 1989). Specifically, a plateau of  $515 \text{ J/m}^2$  was reached for a thin beam, whereas a continuous increase up to values in excess of  $1000 \text{ J/m}^2$  was recorded for a beam a few times thicker. We feel our model is adequate to correlate the delamination  $R$ -curves; an experimental validation is in progress (SPEARING and EVANS, 1990).

## 6. CONCLUDING REMARKS

As illustrated in Fig. 2, two essential features on the  $R$ -curves for slender beams are (a) the plateau  $\mathcal{G}_{ss}$  remains constant for different beam thicknesses, and (b) the steady-state damage zone length  $L_{ss}$  increases with the beam thickness. A family of steady-state, mixed-mode delamination beams is recommended to study large-scale bridging phenomena. Because the  $R$ -curves depend on the specimen geometry, we favor the characterization of materials using bridging laws, instead of the  $R$ -curves. Two experimental procedures are proposed to infer the bridging laws. One requires continuous measurement of the opening of the pre-cut tip and the  $R$ -curve, but does not require any *a priori* knowledge of the bridging law. For the other procedure, the damage response is characterized by a three-parameter spring law, and the parameters are inferred using quantities read from the  $R$ -curve only. From the point of view of structural design, corresponding analyses are needed for other important geometries. The effect of mode mixity merits further study. Elastic anisotropy may play an important role which has been ignored in the present paper. The conception of using large-scale bridging to study localized (plane) damage response requires experimental validation.

## ACKNOWLEDGEMENTS

Discussion with A. G. Evans and S. M. Spearing on experiments has been a great help. Funding was supplied by an ONR/URI contract N-0-0014-86-K-0753, a NSF grant MSS-9011571, and the College of Engineering, the University of California at Santa Barbara. The finite-element computation was performed using ABAQUS.

## REFERENCES

- |  |      |  |
|--|------|--|
| ASHBY, M. F., BLUNT, F. J. and BANNISTER, M. | 1989 | <i>Acta Metall.</i> <b>37</b> , 1847.  |
| BAO, G., FAN, B. and EVANS, A. G.            | 1990 | <i>Mech. Mater.</i> (in press).  |
| BAO, G. and HUI, C.-Y.                       | 1990 | <i>Int. J. Solids Struct.</i> <b>26</b> , 631.   |
| BRADLEY, W. L.                               | 1989 | In <i>Application of Fracture Mechanics to Composite Materials</i> (edited by K. Friedrich), p. 159. Elsevier, New York. |

- BUDIANSKY, B., AMAZIGO, J. C. and EVANS, A. G. 1988 *J. Mech. Phys. Solids* **36**, 167.
- BYUN, J.-H., GILLESPIE, J. W. and CHOU, T.-W. 1990 *J. Composite Mater.* **24**, 497.
- CHAI, H. 1988 *Int. J. Fracture* **37**, 137.
- CHARALAMBIDES, P. G., LUND, J., EVANS, A. G. and McMEEKING, R. M. 1989 *J. appl. Mech.* **56**, 77.
- DE CHARENTENAY, F. X., HARRY, J. M., PREL, Y. J. and BENZEGGAGH, M. L. 1984 In *Effects of Defects in Composite Materials*. ASTM STP **836**, 84.
- DEN HARTOG, J. P. 1987 *Advanced Strength of Materials*. Dover, New York.
- DUGDALE, D. S. 1960 *J. Mech. Phys. Solids* **8**, 100.
- EVANS, A. G. 1990 *J. Am. Ceram. Soc.* **73**, 187.
- HASHEMI, S., KINLOCH, A. J. and WILLIAMS, J. G. 1990 *Proc. R. Soc.* **A427**, 173.
- LIECHTI, K. M. and CHAI, Y.-S. 1990 *J. appl. Mech.* (in press).
- LUCAS, J. P. and ODEGARD, B. C. 1990 In *Advances in Thermoplastic Matrix Composite Materials*. ASTM STP **1044**, 231.
- MAI, Y.-W. and LAWN, B. R. 1986 *A. Rev. Mater. Sci.* **16**, 4159.
- O'BRIEN, T. K. 1987 *J. Am. Helicopter Soc.* **32**, 13.
- OH, T. S., RODEL, J., CANNON, R. M. and RITCHIE, R. O. 1988 *Acta Metall.* **36**, 2083.
- POHANKA, R. C. and SMITH, P. L. 1988 In *Electronic Ceramics, Properties, Devices and Applications* (edited by L. M. Levinson). Marcel Dekker, New York.
- PREL, Y. J., DAVIES, P., BENZEGGAGH, M. L. and DE CHARENTENAY, F. X. 1989 In *Composite Materials: Fatigue and Fracture*, Vol. 2. ASTM STP **1012**, 251.
- REIMANIS, I. E. and EVANS, A. G. 1990 *Acta Metall.* (submitted for publication).
- RICE, J. R. 1968 *J. appl. Mech.* **35**, 379.
- SBAIZERO, O., CHARALAMBIDES, P. G. and EVANS, A. G. 1990 *J. Am. Ceram. Soc.* **73**, 1936.
- SPEARING, S. M. and EVANS, A. G. 1990 *Acta Metall.* (submitted for publication).
- SU, K. B. 1990 In *Advances in Thermoplastic Matrix Composite Materials*. ASTM STP **1044**, 276.
- SUO, Z. 1990 *J. appl. Mech.* **57**, 627.
- SUO, Z., ORTIZ, M. and NEEDLEMAN, A. 1991 Accepted for publication in *J. Mech. Phys. Solids*.
- VARIAS, A. G., SUO, Z. and SHIH, C. F. 1991 *J. Mech. Phys. Solids* **39**, 963.
- VEKINIS, G., ASHBY, M. F. and BEAUMONT, P. W. R. 1990 *Acta Metall.* **38**, 1151.
- ZOK, F. and HOM, C. L. 1990 *Acta Metall.* **38**, 1895.
- WIEDERHORN, S. M., SHORBAND, A. M. and MOSES, R. L. 1968 *J. appl. Phys.* **39**, 1569.